Endorsed by **IPEM** Institute of Physics and Engineering in Medicine   **PURPOSE-LED PUBLISHING™**

PAPER • OPEN ACCESS

Micromagnetic stimulation (µMS) controls dopamine release: an *in vivo* study using WINCS *Harmoni*

To cite this article: Renata Saha *et al* 2025 *Biomed. Phys. Eng. Express* **11** 025058

View the article online for updates and enhancements.

You may also like

- FLASH radiotherapy: technical advances, evidence of the FLASH effect and mechanistic insights
  Mustapha Chaoui, Othmane Bouhali and Yahya Tayalati

- Deep learning-based video-level view classification of two-dimensional transthoracic echocardiography
  Hanlin Cheng, Zhongqing Shi, Zhanru Qi et al.

- Research progress of bioactive glass in the remineralization of dental hard tissue
  Wenhao Wang, Ruhua Chen, Yimeng Xie et al.

Biomedical Physics & Engineering Express

PAPER

OPEN ACCESS

Micromagnetic stimulation (μMS) controls dopamine release: an *in vivo* study using WINCS *Harmoni*

Renata Saha[1] , Abhinav Goyal[2,3] , Jason Yuen[2,4] , Yoonbae Oh[2,5] , Robert P Bloom[1] , Onri J Benally[1] , Kai Wu[1] , Theoden I Netoff[6] , Walter C Low[7] , Kevin E Bennet[2,8] , Kendall H Lee[2,5] , Hojin Shin[2,5,*] and Jian-Ping Wang[1,*]

1   Department of Electrical and Computer Engineering, University of Minnesota, Minneapolis, MN, United States of America
2   Department of Neurologic Surgery, Mayo Clinic, Rochester, MN, United States of America
3   Medical Scientist Training Program, Mayo Clinic, Rochester, MN, United States of America
4   Deakin University, IMPACT—the Institute for Mental and Physical Health and Clinical Translation, School of Medicine, Barwon Health, Geelong VIC 3216, Australia
5   Department of Biomedical Engineering, Mayo Clinic, Rochester, MN, United States of America
6   Department of Biomedical Engineering, University of Minnesota, Minneapolis, MN, United States of America
7   Department of Neurosurgery, University of Minnesota, Minneapolis, MN, United States of America
8   Division of Engineering, Mayo Clinic, Rochester, MN, United States of America
*   Authors to whom any correspondence should be addressed.

E-mail: Shin.Hojin@mayo.edu and jpwang@umn.edu

Abstract

Research into the role of neurotransmitters in regulating normal and pathologic brain functions has made significant progress. Yet, clinical trials that aim to improve therapeutic interventions do not take advantage of the *in vivo* changes in the neurochemistry that occur in real time during disease progression, drug interactions or response to pharmacological, cognitive, behavioral, and neuromodulation therapies. In this work, we used the WINCS *Harmoni* tool to study the real time *in vivo* changes in dopamine release in rodent brains for the micromagnetic neuromodulation therapy. Although still in its infancy, micromagnetic stimulation (μMS) using micro-meter sized coils or microcoils (μcoils) has shown incredible promise in spatially selective, galvanic contact free and highly focal neuromodulation. These μcoils are powered by a time-varying current which generates a magnetic field. As per Faraday's Laws of Electromagnetic Induction, this magnetic field induces an electric field in a conducting medium (here, the brain tissues). We used a solenoidal-shaped μcoil to stimulate the medial forebrain bundle (MFB) of the rodent brain *in vivo*. The evoked *in vivo* dopamine releases in the striatum were tracked in real time by carbon fiber microelectrodes (CFM) using fast scan cyclic voltammetry (FSCV). Our experiments report that μcoils can successfully activate the MFB in rodent brains, triggering dopamine release *in vivo*. We further show that the successful release of dopamine upon micromagnetic stimulation is dependent on the orientation of the μcoil. Furthermore, varied intensities of μMS can control the concentration of dopamine releases in the striatum. This work helps us better understand the brain and its conditions arising from a new therapeutic intervention, like μMS, at the level of neurotransmitter release. Despite its early stage, this study potentially paves the path for μMS to enter the clinical world as a precisely controlled and optimized neuromodulation therapy.

1. Introduction

Chemical signaling mediated by an intricate balance of specific neurotransmitters is necessary for normal functioning of the brain. Diseases, injuries, or new therapeutic interventions could disrupt this balance of neurotransmitters, and the results can be devastating. For instance, low dopamine levels are linked to the following medical conditions—anxiety, depression, tremors, fatigue, and cognitive imbalance [1–6]. In a

similar context, low levels of serotonin are associated with insomnia, migraine headaches, and suicidal ideation among other conditions [7–9]. These and other brain disorders associated with neurotransmitter imbalance affect one billion people globally [10]. Therefore, accurate measurement of these neurotransmitter concentrations in patients during the onset of diseases, recovering from injuries or testing new therapies is of utmost importance [11].

Microdialysis is widely used for measuring neurochemical concentrations with high selectivity and specificity [12, 13]. However, this technique has drawbacks when compared to electrochemical methods such as fast-scan cyclic voltammetry (FSCV) in terms of its large microdialysis probe size (>200 μm) and limited temporal resolution (<1 min) [14–16]. Electrochemical techniques such as FSCV are well suited for measuring extracellular dopamine concentrations in real time with much better spatiotemporal resolutions (~milliseconds) and detection sensitivity (<5 nM). The carbon fiber microelectrode (CFM) probe used in FSCV is of much smaller diameter (<10 μm), causing less damage to brain tissues compared to microdialysis probes. The voltage applied to the CFM is initially kept at a fixed resting potential and then gradually ramped up to an electric potential necessary to oxidize and reduce electroactive species (e.g. dopamine) before the potential is returned to the resting potential again [17]. This voltage sweep is fast (<10 ms) and is repeated every 100 ms (equivalent to a scanning frequency of 10 Hz). The voltammogram provides a chemical signature which is unique to the electroactive species (dopamine, serotonin, acetylcholine etc) and can be used to study their phasic changes in extracellular concentrations.

Neuronal dopamine release from the mammalian midbrain can be distinctly characterized into 2 patterns: tonic activity and phasic burst activity [18]. Tonic activity is observed when extrasynaptic dopamine is released spontaneously by pacemaker-like firing of midbrain neurons into the striatum. This modulates behavioral flexibility by maintaining a relatively homeostatic extracellular concentration of dopamine. Whereas during phasic burst activity, transient dopamine is released at the synapse, triggering neural plasticity. FSCV is a technique well suited to measuring these phasic changes in dopamine or other neurotransmitter concentrations. It is a differential technique, in which large capacitive currents at the CFM surface must be subtracted to resolve the Faradaic current for precise voltammetric measurements [18].

Micromagnetic neurostimulation was first experimentally implemented in an *ex vivo* study on rabbit retinal neurons using commercially available solenoidal-shaped microcoils (μcoils) [19]. Since then, attempts have been made by several groups to use similar μcoil prototypes in several experimental settings, both *in vitro* and *in vivo*, to showcase the efficacy of micromagnetic neurostimulation [20–25]. Furthermore, different designs of μcoils, solenoidal [20], planar [22, 26], V-shaped [27] or trapezoidal [27], with or without soft magnetic material cores [28], have been investigated. In this neuromodulation technique, μcoils are the devices that are powered by time-varying currents at varying amplitudes, pulse widths (PW) and frequencies. According to Faraday's Laws of Electromagnetic Induction, these current carrying μcoils generate a magnetic field, which in turn induces an electric field on a conducting surface (here, biological conductors such as neural tissues). Since the induced electric field that activates the neural tissues are not in direct galvanic contact with the tissues, these μcoils exhibit less implant surface corrosion due to biofouling [29]. The induced electric field is highly directional in nature causing spatially-selective activation of the neural tissue from these μcoils [20]. Furthermore, in a recent numerical study, these μcoils have shown significantly less radio frequency (RF) heating (antenna effect) from a 1.5 Tesla magnetic Resonance Imaging (1.5T-MRI) environment compared to traditional deep brain stimulation (DBS) leads [30]. Therefore, these μcoils are MRI-safe, enabling patients with these implants to undergo an MRI scan after insertion of these μcoil implants in their brains.

Micromagnetic neurostimulation is quite recent in its origin and is still in its infancy. Tremendous efforts are yet to be made to develop the μcoils to be fit for testing on non-human primates to gradually progress them into clinical trials. Being a relatively new neuromodulation therapy, a study on the associated neurotransmitter releases is required. In this work, we studied how micromagnetic stimulation of the substantia nigra-striatal nerve fibers in the medial forebrain bundle (MFB) in a rodent brain releases dopamine *in vivo*. Upon stimulation from the μcoils, we quantified the phasic dopamine responses in real time from the striatum using FSCV. This work is a proof-of-concept study on rodent brains *in vivo*, demonstrating the feasibility of μcoils in activating the MFB fibers and the neuronal dopaminergic pathway thereby quantifying the dopamine release from the striatum.

2. Materials and methods

2.1. The μcoil probe fabrication
In this *in vivo* study, we used the Magnetic Pen (MagPen) as the μcoil implant (μcoil dimension = 1 mm × 0.6 mm × 0.5 mm) [20, 21]. The commercially available solenoidal μcoil of model no. TDK Corporation MLG1005SR10JTD25 was soldered at the tip of the green printed circuit board (PCB) of length 3 cm. To minimize brain tissue damage during implantation of the MagPen probe, the thickness of the PCB was reduced to 0.4 mm. To determine if the MagPen orientation with respect to the MFB fibers in the

rodent brain affected dopamine release from the striatum, we fabricated the prototype in two orientations: Type <u>H</u>orizontal (Type H or MagPen-Type H) and Type <u>V</u>ertical (Type V or MagPen-Type V) (see figure S1(a)). The width of the μcoil tips for MagPen-Type H and MagPen-Type V were optimized to be at 1.7 mm and 1.4 mm respectively. The complete image of the MagPen prototype has been reported in figure S1(b) (see Supplementary Information S1). To ensure complete biocompatibility in addition to an antileakage current and waterproof sealing for the probe, the tip of the MagPen was encapsulated in a 10 μm thick coating of Parylene-C (SCS-Labcoater Parylene-C deposition system). Successful coating for the MagPen prototype was determined once the impedance between the MagPen and a salt bath was >5MΩ [20, 21].

2.2. The electrical circuit characterization of the μcoil

Resistance (R), inductance (L) and capacitance (C) values of the μcoil implant were measured using an LCR meter (Model no. BK Precision 889B; see table S1 in Supplementary Information S1) at two frequencies (120 Hz and 1 kHz). The frequency of operation for the μcoil in this work was around 60–130 Hz compared to other reported works with MagPen where the frequency of operation for the μcoil was at 1–5 kHz [20, 21]. The frequency of operation around 60–130 Hz contributed to the benefit for micromagnetic operation on MFB fibers in the rodent brain as compared to the LCR meter measurements at 1 kHz. The DC resistance (R_{DC}), the series inductance (L_s) and the parallel capacitance (C_p) values remained almost the same for both frequency measurements (120 Hz and 1 kHz; see table S1). The series capacitance (C_s) value increased, and the parallel inductance (L_p) value decreased by several orders (see table S1) at 120 Hz. Therefore, reactance from C_s (X_{CS}) offered lower resistance to the current flow in the series RL branch and L_p offered higher resistance to the parallel LC branch (X_{Lp}) resulting in complete flow of current through the series RL branch of the μcoil (see figure S1(c)). Therefore, the μcoil in MagPen acted as a series RL circuit (see figure S1(c)).

The induced electric field in micromagnetic activation of neurons is a function of L_s. The electromotive force (emf or $v(t)$) induced in the neural tissues is expressed as: $v(t) = L_s \frac{di(t)}{dt}$. This emf is generated due to a time-varying magnetic field ($\boldsymbol{B(t)}$) as per Faraday's Laws of Electromagnetic Induction and $\frac{di(t)}{dt}$ is the time derivative of the time-varying current ($\boldsymbol{i(t)}$) through the inductor or μcoil. This has been used to study the effect of micromagnetic neurostimulation on the MFB fibers of the rat brain to trigger dopamine release in rats (see section 3.2). The resistance (R) contributes to the Joule heating on the neural tissues from the μcoil (*heat dissipated* = $i(t)^2 R_{DC} t$). Our numerical calculations and independent experiments

corroborate with existing literature which report that the temperature increase from these μcoils on neural tissues upon micromagnetic stimulation remains below 1 °C [21, 22, 25].

2.3. Fabrication of carbon fiber microelectrode (CFM)

Carbon fiber microelectrodes (CFMs) (see figure 1(a-i)) were fabricated using a standardized design at Mayo Clinic, Rochester, MN [31, 32]. The microelectrode involved isolating and inserting a single carbon fiber (AS4, diameter = 7 μm; Hexcel, Dublin, CA) into a silica tube (inner diameter (ID) = 20 μM, outer diameter (OD) = 90 μM OD, 10 μM thick coating with polyimide; Polymicro Technologies, Phoenix, AZ). The connection between the carbon fibers extending out of the silica tubing were sealed with epoxy resin. The carbon fiber in the silica tubing was then connected to a conductive wire composed of nitinol (Nitinol #1, an alloy of nickel and titanium; Fort Wayne Metals, IN) coated with a silver-based conductive paste [31]. The carbon fiber attached nitinol wire was then insulated with a polyimide tube (0.0089″ ID, 0.0134″ OD, 0.00225″ WT; Vention Medical, Salem, NH) up to the carbon fiber sensing tip. The exposed carbon fiber was then trimmed under a dissecting microscope to a length of ~50 μm. Teflon-coated silver (Ag) wire (A-M systems, Inc., Sequim, WA) was prepared as an Ag/AgCl counter-reference electrode by chlorinating the exposed tip in saline with a 9 V dry cell battery. CFM was pretested *in vitro* in a TRIS buffer (15 mM tris, 3.25 mM KCl, 140 mM NaCl, 1.2 mM $CaCl_2$, 1.25 mM NaH_2PO_4, 1.2 mM $MgCl_2$, and 2.0 mM Na_2SO_4, with the pH adjusted to 7.4) [33] prior to implantation.

2.4. Implantation of CFM and MagPen *in vivo*

The rat (Sprague Dawley, male, 250 g, Envigo, United States) was anesthetized with urethane (1.5 g kg^{-1} i.p.; Sigma-Aldrich, St Louis, MO, USA) and administered buprenorphine (0.05–0.1 mg kg^{-1} s.c., Par Pharmaceutical, Chestnut Ridge, NY, USA) for analgesia. Upon complete anesthesia, rats were placed in a stereotaxic frame (David Kopf Instruments, Tujunga, CA, USA) with its body resting on a heating pad (41 °C). Respiratory rate (RespiRAT, Intuitive Measurement Systems), hind-paw and tail pinch were used to monitor the physiological state and depth of anesthesia over the entire course of the experiment. Using a standard rat atlas [34], three trephine holes were drilled, the first for placement of a CFM into the striatum (AP 1.2 mm from bregma, ML 2.0 mm, and DV −5.1 mm from dura) (see figure 1(a-i)), the MagPen into the medial forebrain bundle (MFB) (AP −4.6 mm from bregma, ML 1.3 mm, and DV −9 mm from dura) (see figure 1(a-ii)), and a third for an Ag/AgCl reference/counter electrode into the contralateral cortex [35]. The animal study was reviewed and approved by the Institutional Animal Care and Use
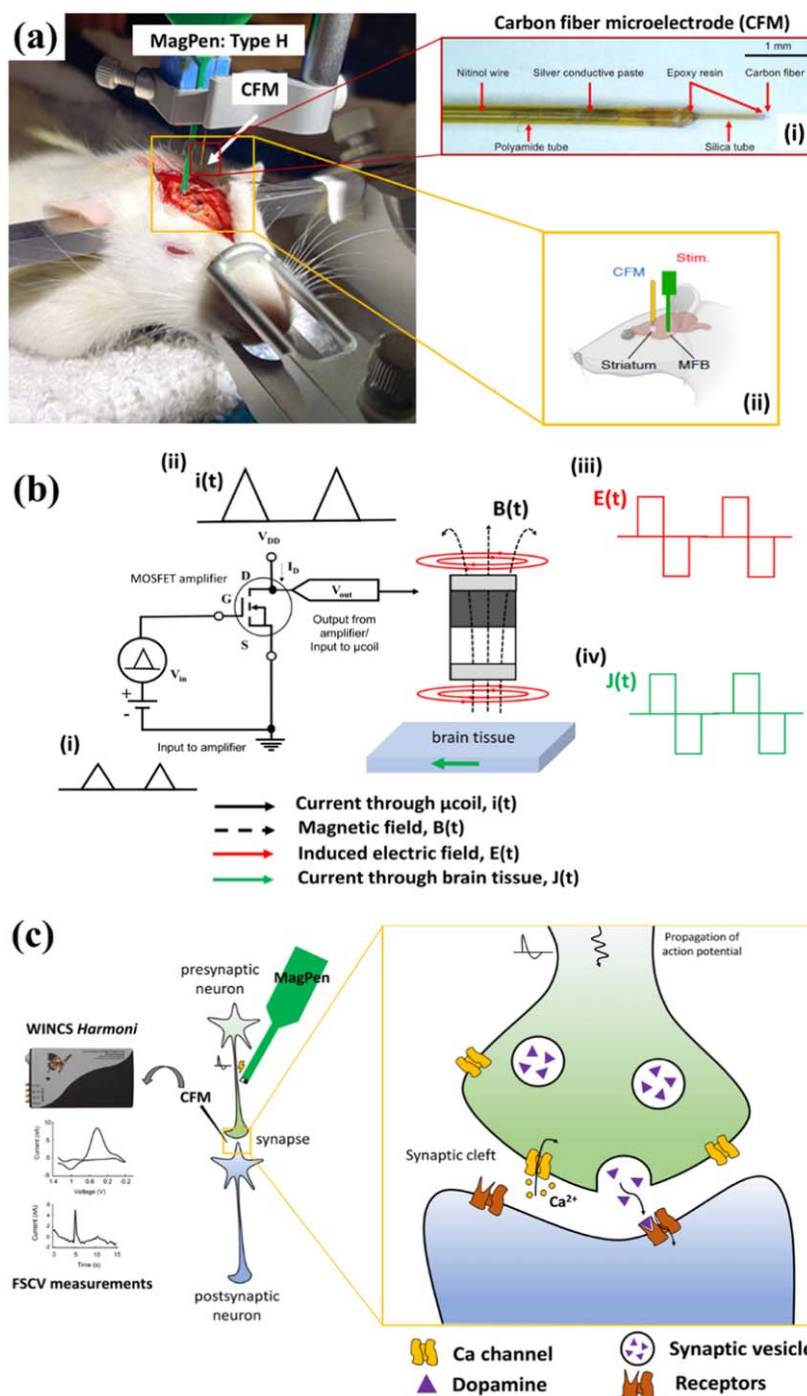
Figure 1. (a) *in vivo* experimental set-up where the MagPen is inserted into the medial forebrain bundle (MFB) and the carbon fiber microelectrode (CFM) is inserted into the striatum. (i) The zoom-in image of the CFM with its different parts labelled. (ii) Schematic overview of the regions of the brain being stimulated and recorded. Partially created with BioRender.com Rojas cabrera, J. (2025) https://BioRender.com/f80x888. (b) (i-iv) The signal flowchart through which the MFB is being stimulated by the MagPen-Type H. (c) Schematic overview of MagPen stimulation and the CFM electrode is positioned in the extracellular space that records dopamine spillover from synaptic clefts in the vicinity. Upon MagPen stimulation of the MFB, dopamine release is evoked in the dorsal striatum. This release is measured by the CFM linked with WINCS *Harmoni*.

Committee (IACUC), Mayo Clinic, Rochester, MN. Protocol No.: A00003894.

2.5. The MagPen driving circuitry

A function generator (Model no. RIGOL DG1022Z) is used to generate bursts of triangular waveforms. To produce the required drive current, these voltage waveforms are amplified by a Class-D amplifier (Model no. Pyramid PB717X) set at a constant gain A (see figure 1(b-ii)). This amplified voltage is applied across the μcoil, resulting in the current ($i(t)$) (denoted by solid-black colored lines in figure 1(b-i)). Using the trigger function in the function generator, the total stimulation time span and the wait time between each successive stimulation trial was controlled.

Table 1. Modeling parameters for electrical electrode.

Parameter description	Value
Wire diameter (stainless steel)	0.127 mm
Separation between 2 wires	1 mm
Length (not covered by polyimide coating)	1 mm
Tissue dimension (L × W × H)	2 mm × 2 mm × 300 μm
Conductivity of tissue (σ)	0.13 S m^{-1}
Air dimension (L × W × H)	5 mm × 5 mm × 4 mm
Energy error (user-specified)	1%
Final solution no. of mesh elements	200,000
Adaptive passes (converged)	6

Table 2. Modeling parameters for the μcoil.

Parameter description	Value
μcoil dimension (L × W × H)	1 mm × 600 μm × 500 μm
no. of turns (N)	21
Wire diameter	7 μm
Tissue dimension (L × W × H)	4 mm × 4 mm × 300 μm
Conductivity of tissue (σ)	0.13 S m^{-1}
Air dimension (L × W × H)	10 mm × 10 mm × 4 mm
Energy error (user-specified)	1%
Final solution no. of mesh elements	410,000
Adaptive passes (converged)	6

2.6. WINCS *harmoni* for *in vivo* neurotransmitter recording

WINCS *Harmoni* [11] is a closed-loop neurochemical monitoring system that can monitor real-time changes in neurotransmitter levels upon *in vivo* stimulation. This research platform is a very convenient research tool that helps track changes in the brain process during disease progression and its response to pharmacologic, cognitive, behavioral and neuromodulation therapies by directly studying the brain chemistry.

2.7. Finite element modeling (FEM) of the neural implants

The bipolar twisted electrodes for *in vivo* electrical stimulation (Model no. Plastics One, MS 303/2, Roanoke, VA, USA) were modeled on ANSYS-Maxwell, electrostatic solver to compare the electric field contour plots between electrical and micromagnetic stimulation. The twisted electrode dimensions, tissue slab parameters, boundary conditions and the high-resolution tetrahedral mesh size used are detailed in table 1. FEM simulations on Ansys-Maxwell, eddy current solver [36] (ANSYS, Canonsburg, PA, United States) were used to study the magnetic field and the induced electric field from the μcoils. It solves an advanced form of the T-Ω formulation of the Maxwell's equations [37]. The ceramic core μcoil dimensions, tissue slab parameters, boundary conditions and the high-resolution tetrahedral mesh size used are detailed in table 2. All simulations were done using the Minnesota Supercomputing Institute (MSI) at the University of Minnesota (8 cores of Intel Haswell E5–2680v3 CPU, $64 \times 8 = 512$ GB RAM and 1 Nvidia Tesla K20 GPU). The induced electric field values were then exported to be analyzed using a customized code written in MATLAB (The Mathworks, Inc., Natick, MA, USA).

3. Results

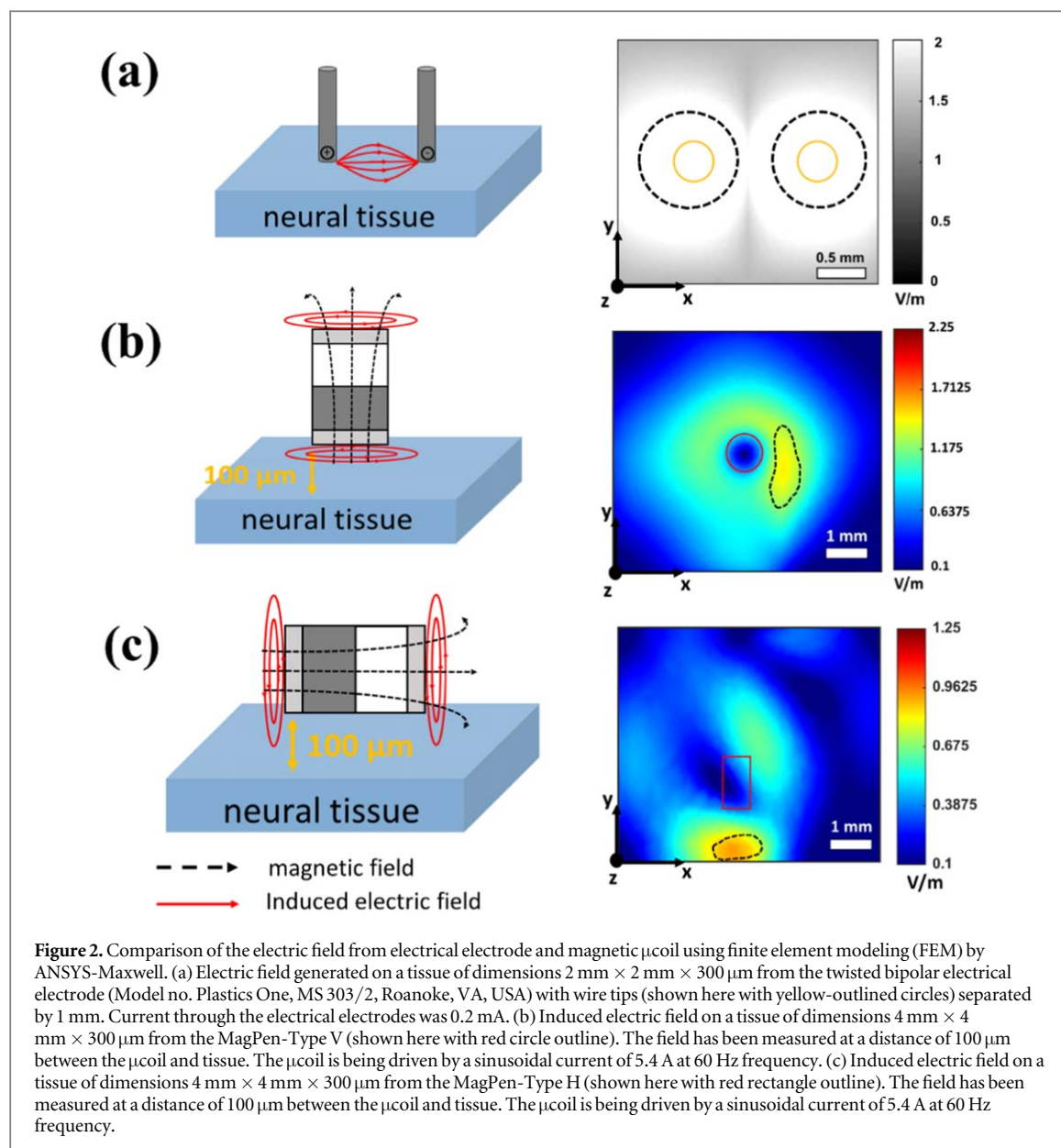### 3.1. μMS of MFB fibers and FSCV measurements from the striatum

In this work the MagPen: Type Horizontal (Type H or MagPen-Type H) activated the MFB fibers (see figure 1(a)) and the CFM.WINCS *Harmoni* [11] was used to track the evoked *in vivo* dopamine release from the striatum using FSCV (see figures 1(a-i) and (a-ii)). The MagPen driving circuitry and the associated waveforms are demonstrated in the following signal flowchart (see figure 1(b)). A function generator (Model no. RIGOL DG1022Z) is used to generate bursts of triangular waveforms. This is the current through the μcoil (*i*(*t*)) (denoted by solid-black colored lines in figure 1(b-i)). Then the current *i*(*t*) is amplified by a Class-D amplifier (Model no. Pyramid PB717X) set at a constant gain A (see figure 1(b-ii)). This time-varying current through a μcoil generates a time-varying magnetic field (*B*(*t*)) (represented by black-dotted lines in figure 1(b)). As per Faraday's Law of Electromagnetic Induction, this time-varying magnetic field induces an electric field (*E*(*t*)) (represented by solid-red lines in figure 1(b-iii)) which is used to activate the MFB fibers. This follows directly from the equation: $\oint \boldsymbol{E(t)} \cdot d\boldsymbol{l} = -\iint \frac{\partial \boldsymbol{B(t)}}{\partial t} \cdot d\boldsymbol{S}$. Therefore, we obtain: $\boldsymbol{E(t)} \propto \frac{d\boldsymbol{B(t)}}{dt} \propto \frac{d\boldsymbol{i(t)}}{dt}$. Hence, on applying bursts of triangular current waveform (*i*(*t*)) through the μcoil, we will obtain an induced electric field waveform (*E*(*t*)) in the form of bursts of a biphasic square waveform (see solid-red lines in figure 1(b-iii)). As this induced electric field activates the MFB fibers, it will induce a biphasic square current, *J*(*t*) (represented by solid green lines) in the MFB fibers, thereby activating them (see figure 1(b-iv)). More details on the specifics of the triangular waveform that triggers dopamine release can be found in section 3.3.

Upon stimulation from the μcoils in the MagPen, due to propagation of action potentials along MFB axons, depolarization takes place at post-synaptic striatal dopaminergic neurons. This is followed by the influx of Ca-ions through voltage-gated calcium ion channels (see figure 1(c)) triggering exocytosis of dopamine-containing vesicles. The CFM with the assistance of WINCS *Harmoni* tracks this evoked neurotransmitter (in this case, dopamine) release using FSCV (see figure 1(c)).

3.2. Simulation study of electric field for dopamine release upon electric and micromagnetic stimulation of the MFB fibers
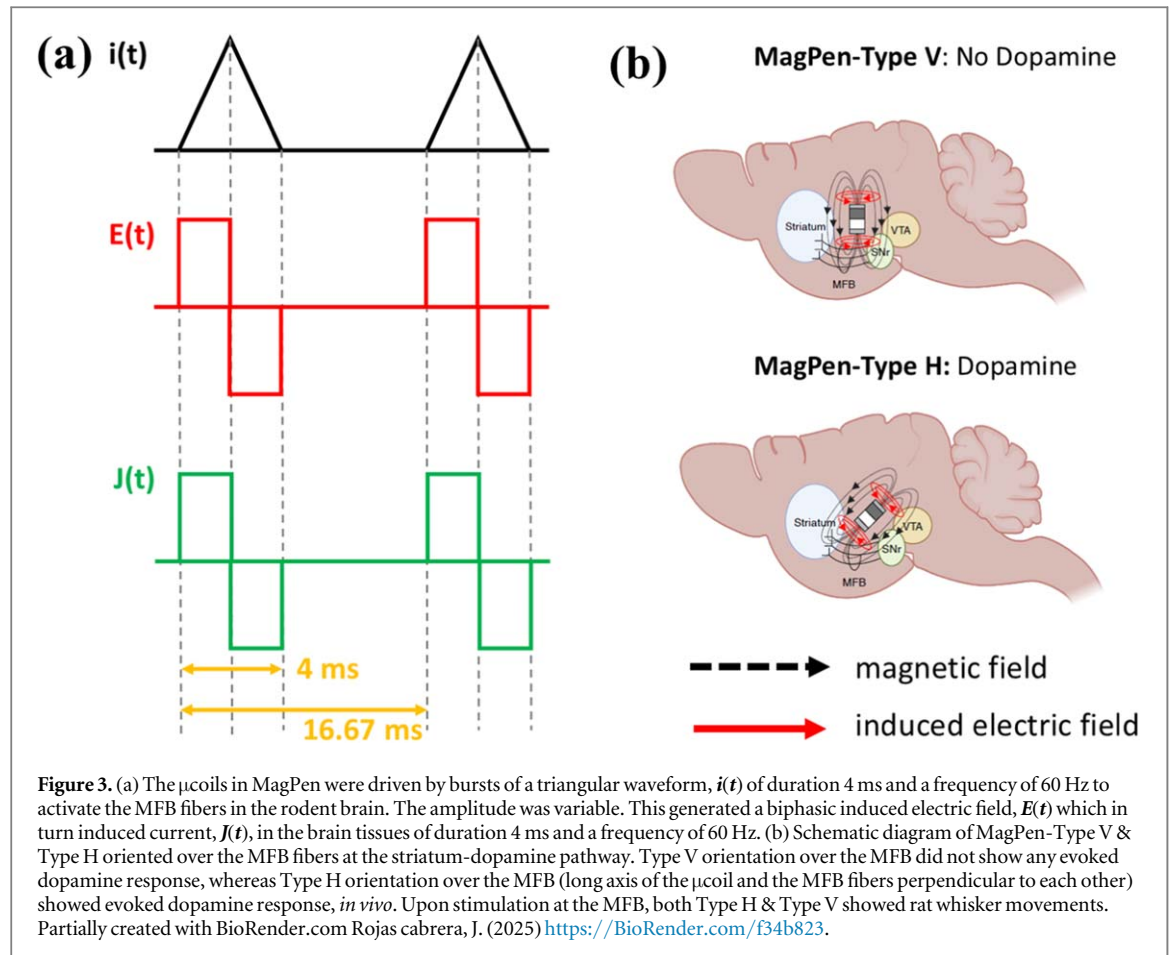
In previous studies on evoked dopamine release upon MFB stimulation using electrical stimulation *in vivo*, 2

Figure 2. Comparison of the electric field from electrical electrode and magnetic μcoil using finite element modeling (FEM) by ANSYS-Maxwell. (a) Electric field generated on a tissue of dimensions 2 mm × 2 mm × 300 μm from the twisted bipolar electrical electrode (Model no. Plastics One, MS 303/2, Roanoke, VA, USA) with wire tips (shown here with yellow-outlined circles) separated by 1 mm. Current through the electrical electrodes was 0.2 mA. (b) Induced electric field on a tissue of dimensions 4 mm × 4 mm × 300 μm from the MagPen-Type V (shown here with red circle outline). The field has been measured at a distance of 100 μm between the μcoil and tissue. The μcoil is being driven by a sinusoidal current of 5.4 A at 60 Hz frequency. (c) Induced electric field on a tissue of dimensions 4 mm × 4 mm × 300 μm from the MagPen-Type H (shown here with red rectangle outline). The field has been measured at a distance of 100 μm between the μcoil and tissue. The μcoil is being driven by a sinusoidal current of 5.4 A at 60 Hz frequency.

mA of biphasic square current waveforms of duration 4 ms and frequency ranging between 60–130 Hz were applied through the electrode [32]. The goal was to determine the amplitude of the current through the μcoils that can generate an induced electric field value similar to the electric field generated from electrical stimulation *in vivo*. Using ANSYS-Maxwell (electrostatic solver), we studied the electric field contour plot from the bipolar twisted electrodes (Model no. Plastics One, MS 303/2, Roanoke, VA, USA) upon being driven by 0.2 mA of current (see figure 2(a)). The circular wire tips of diameter 0.127 mm separated by 1 mm have been denoted with yellow circles (see figure 2(a)). The electric field has been simulated on a tissue of dimension 2 mm × 2 mm × 300 μm. Since the electrodes are in direct electrochemical contact with the tissues during neuromodulation, in this FEM-modeling study in figure 2(a) (see table 1 for the detailed modeling parameters), the distance between

the electrical electrode and the biological tissue was negligible.

The magnetic μcoils were also numerically simulated on ANSYS-Maxwell (eddy current solver) to match the induced electric field values to that of the electric field values reported in figure 2(a). Since the μcoils are not in direct electrochemical contact with the brain tissues (due to the insulating coating), we have simulated a distance of 100 μm between the μcoils and the biological tissue of dimension 2 mm × 2 mm × 300 μm. Figure 2(b) shows the induced electric field contour plot when the μcoil of the MagPen is oriented in the Type V orientation with respect to the tissues. Figure 2(c) shows the electric field contour plots when the μcoil of the MagPen is oriented in the MagPen-Type H orientation with respect to the tissues. It was investigated through FEM modeling that a sinusoidal current of amplitude 5.4 A at a frequency of 60 Hz was necessary to drive the μcoil such that it

Figure 3. (a) The μcoils in MagPen were driven by bursts of a triangular waveform, *i(t)* of duration 4 ms and a frequency of 60 Hz to activate the MFB fibers in the rodent brain. The amplitude was variable. This generated a biphasic induced electric field, *E(t)* which in turn induced current, *J(t)*, in the brain tissues of duration 4 ms and a frequency of 60 Hz. (b) Schematic diagram of MagPen-Type V & Type H oriented over the MFB fibers at the striatum-dopamine pathway. Type V orientation over the MFB did not show any evoked dopamine response, whereas Type H orientation over the MFB (long axis of the μcoil and the MFB fibers perpendicular to each other) showed evoked dopamine response, *in vivo*. Upon stimulation at the MFB, both Type H & Type V showed rat whisker movements. Partially created with BioRender.com Rojas cabrera, J. (2025) https://BioRender.com/f34b823.

could generate an induced electric field on a biological tissue located 100 μm away, of similar orders of magnitude as that from electrical stimulation (see figure 2(c)).

Upon comparing the electric field contour plots from figures 2(a)–(c), we have shown how much more spatially specific the μcoil is compared to the electrical stimulation electrodes. In figure 2(a), the spatially uniform field of activation around the electrode tips spans in cylindrical blocks of volume ~0.24 mm³, each. That calculates to 40% of the tissue volume which has the maximum probability of activation with the threshold electric field being around 1.8–2 V mm⁻¹ (denoted by black-dotted lines in figure 2(a)). Whereas in figures 2(b) and (c), only 1.13 mm³ and 0.63 mm³ of the tissue volume out of 4.8 mm³ (denoted by black-dotted outlines) has maximum potential of getting activated by MagPen-Type V & MagPen-Type H, respectively. This calculates to a spatial specificity of ~24% and 13% of the tissue volume for MagPen-Type H and MagPen-Type V prototypes, respectively (see figures 2(b) and (c)). If one rotates the μcoil in a clockwise or in an anticlockwise direction keeping the tissue location constant, it will activate a completely different volume of tissue. Since the induced electric field values in the spatial contour plots are greater for MagPen-Type V, it might be a common notion that Type V would successfully activate the MFB fibers and Type H

will not. However, our experiments show that Type H successfully activated MFB fibers whereas Type V did not. Herein lies the importance of directionality of the induced electric field in successfully activating the MFB fibers. In section 3.4, we have discussed the clinical significance of this directionality and/or orientation dependence of magnetic μcoils with respect to the neural fibers.

3.3. Current waveform driving the μcoil in MagPen to activate the MFB fibers

Previous reports suggest that a current (*J(t)*, see figure 3(a)) of amplitude 300 μA in the shape of a biphasic square of duration 4 ms (=2 ms duration in each phase) and frequency 60–130 Hz needs to be injected into neural tissues to evoke dopamine release *in vivo* when the MFB fibers are activated by an electrical stimulation [17, 33, 38]. Keeping this as the standard, we tried to deliver appropriate current waveforms through the μcoil (*i(t)*, see figure 3(a)) in the MagPen such that we can correlate the evoked dopamine response from micromagnetic stimulation to that of electrical stimulation *in vivo*. The amplitudes of the induced electric field necessary to activate the MFB for potential dopamine release has been numerically calculated in figure 2. We have shown how variation of this amplitude of the current through the μcoil influences the evoked dopamine release from the

striatum in section 3.5. This section focuses more on the duration and frequency components of the current through the µcoils.

The µcoils in MagPen being driven by a time-varying current, $i(t)$ generates a magnetic field, $\boldsymbol{B}(t)$ which is given by equation (1):

$$\boldsymbol{B}(t) = \frac{\mu_r \mu_0 i(t) N}{L} \tag{1}$$

where μ_r is the relative permeability of the medium, μ_0 is the vacuum permeability, N is the number of turns of the µcoil and L is the length of the µcoil. figure S3 of Supplementary Information S3 contains the spatial contour graph for the magnetic flux density $(\boldsymbol{B_{x,y,z}})$. However, from equation (1) it is evident that the temporal component of the magnetic field is equivalent to that of the current driving the µcoil.

Following the rules of Faraday's Law of Electromagnetic Induction, this time-varying current induces an electric field on a conductive medium, which, in this work, is the brain. This induced electric field can be expressed by equation (2):

$$\oint \boldsymbol{E} \cdot d\boldsymbol{l} = -\iint \frac{\partial \boldsymbol{B}(t)}{\partial t} \cdot d\boldsymbol{S} \tag{2}$$

where $\boldsymbol{B}(t)$ is the magnetic field generated from the µcoil, $\boldsymbol{E}$ is the induced electric field activating the neurons, and $\boldsymbol{l}$ and $\boldsymbol{S}$ are the contour and the surface area of the neural tissue.

Upon substituting the value of $\boldsymbol{B}(t)$ from equation (1) in equation (2), we get the following in equation (3):
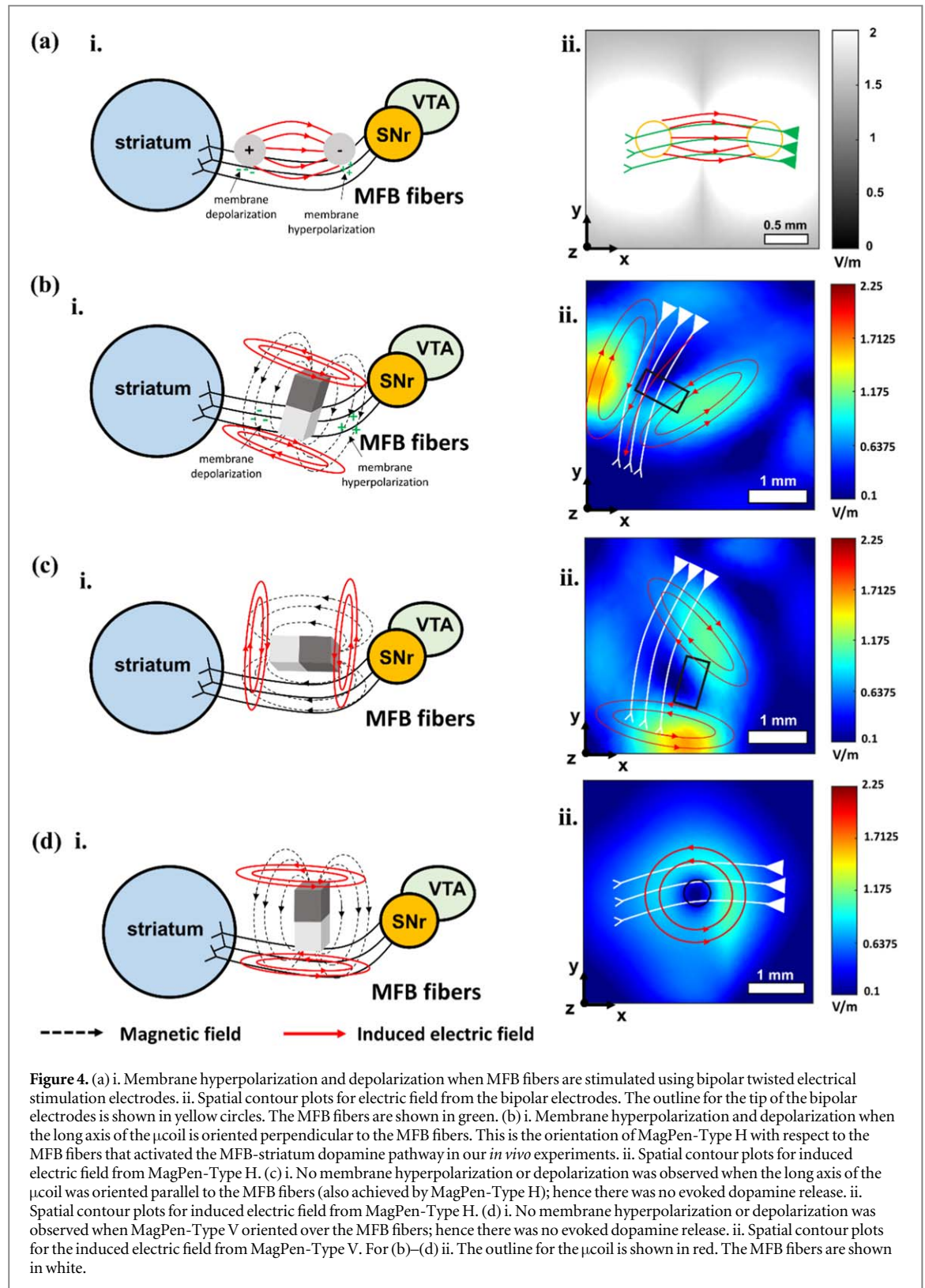
$$\oint \boldsymbol{E} \cdot d\boldsymbol{l} = -\frac{\mu_r \mu_0 N}{L} \cdot \frac{di(t)}{dt} \iint d\boldsymbol{S} \tag{3}$$

Therefore, we get that the required induced electric field for neural activation from the µcoil is a first order time-derivative of the time-varying current through the µcoil. Recalling our previous statement in this section, we required the current through the neural tissues to be a biphasic square waveform ($\boldsymbol{J}(t)$, represented by solid-green lines in figure 3(a)) of duration 4 ms and frequency 60 Hz. This means that the induced electric field also needs to be a biphasic square waveform of the exact same duration and frequency ($\boldsymbol{E}(t)$, represented by solid-red lines in figure 3(a)). Since $\boldsymbol{E}(t) \propto \frac{di(t)}{dt}$, the current ($i(t)$) through the µcoil needs to be a triangular waveform of the same duration and frequency shown in solid-black line in figure 3(a). To summarize, we applied 1-cycle bursts of a triangular current waveform of duration 4 ms; each burst was repeated at a frequency of 60 Hz, meaning each burst was separated by a duration of 12.667 ms. The total stimulation applied was for a time span of 2 s (trigger controlled by the function generator) and a wait time of 5 min was applied between each successive trial.

3.4. Orientation of the µcoil with respect to the MFB fibers for evoked dopamine release *in vivo*

The correct orientation of the µcoil with respect to neural tissues has been quite a debated topic for the micromagnetic neurostimulation technology [19, 20, 23, 25]. In addition to the spatially specific nature of micromagnetic stimulation (discussed in section 3.1), such directional activation provides a significant advantage of micromagnetic neurostimulation over electrical stimulation. As depicted in figure 3(b), MagPen-Type V orientation over the MFB fibers did not evoke dopamine release *in vivo*, whereas Type H orientation over the MFB fibers did. Surprisingly, both Type V and Type H orientations showed rat whisker movements upon *in vivo* stimulation at the MFB. This is because for whisker movements, only a certain amplitude of electric field is necessary to be applied to the motor cortex of the brain. The fact that we observed whisker movements for both MagPen-Type H and MagPen-Type V, it confirmed that both Type H and Type V prototypes generated induced electric field (see figure 2). However, for successful striatal dopamine release upon MFB stimulation, as discussed later in this section, the directionality of the induced electric field is important. Although the anatomical pathway involved in generating and sensing rat whisker movements is not the primary focus of this work, it was used as a metric to figure out whether the electric field was being applied to the MFB of the rat brain [39].

Figure 4 provides an explicit explanation for such µcoil-orientation dependent dopamine release from the rat striatum. The way the µcoil is oriented with respect to the MFB fibers play a critical role in determining successful activation of the MFB fibers. The successful activation upon any kind of external stimulation depends on the neuron membrane hyperpolarization and depolarization effect [40]. During electrical stimulation using bipolar electrodes, one electrode terminal being positive and the other being negative causes membrane depolarization and membrane hyperpolarization on the MFB fibers respectively (see figure 4(a-i)). External current that flows into the membrane hyperpolarize the membrane (since it makes the extracellular side more positive), current that flow out of the membrane probably depolarize it (since it makes the intracellular side more positive). Hence, this activates the MFB fibers to release dopamine into the striatum. The phenomenon is better explained with the electric field spatial contour plots and directionality of the electric field in figure 4(a-ii). Similarly, when the long axis of the µcoil is oriented perpendicular to the MFB fibers (this is achieved by MagPen-Type H), the directionality of the induced electric field is like that of the bipolar electrical electrodes (see figure 4(b-i)). The MagPen-Type H could also be oriented over the MFB fibers such that the long axis of the µcoil is parallel to the MFB fibers (see figure 4(c-i)). However, the

Figure 4. (a) i. Membrane hyperpolarization and depolarization when MFB fibers are stimulated using bipolar twisted electrical stimulation electrodes. ii. Spatial contour plots for electric field from the bipolar electrodes. The outline for the tip of the bipolar electrodes is shown in yellow circles. The MFB fibers are shown in green. (b) i. Membrane hyperpolarization and depolarization when the long axis of the μcoil is oriented perpendicular to the MFB fibers. This is the orientation of MagPen-Type H with respect to the MFB fibers that activated the MFB-striatum dopamine pathway in our *in vivo* experiments. ii. Spatial contour plots for induced electric field from MagPen-Type H. (c) i. No membrane hyperpolarization or depolarization was observed when the long axis of the μcoil was oriented parallel to the MFB fibers (also achieved by MagPen-Type H); hence there was no evoked dopamine release. ii. Spatial contour plots for induced electric field from MagPen-Type H. (d) i. No membrane hyperpolarization or depolarization was observed when MagPen-Type V oriented over the MFB fibers; hence there was no evoked dopamine release. ii. Spatial contour plots for the induced electric field from MagPen-Type V. For (b)–(d) ii. The outline for the μcoil is shown in red. The MFB fibers are shown in white.

directionality of the induced electric field for figure 4(c-i) is such that it does not support membrane hyperpolarization and depolarization that could activate the MFB fibers. Therefore, although the contour plots for the induced electric field is same for both figures 4(b-ii) and (c-ii) cases, the directionality of the induced electric field for the orientation in figure 4(c) does not support MFB activation, whereas

that in figure 4(b) does. When MagPen-Type V is oriented over the MFB fibers, the induced electric field directionality forms a closed circuit that is unable to activate the MFB fibers (see figures 4(d-i) and (d-ii)). This is the reason why we saw evoked dopamine release from the striatum with MagPen-Type H and not with MagPen-Type V stimulation over the MFB fibers.
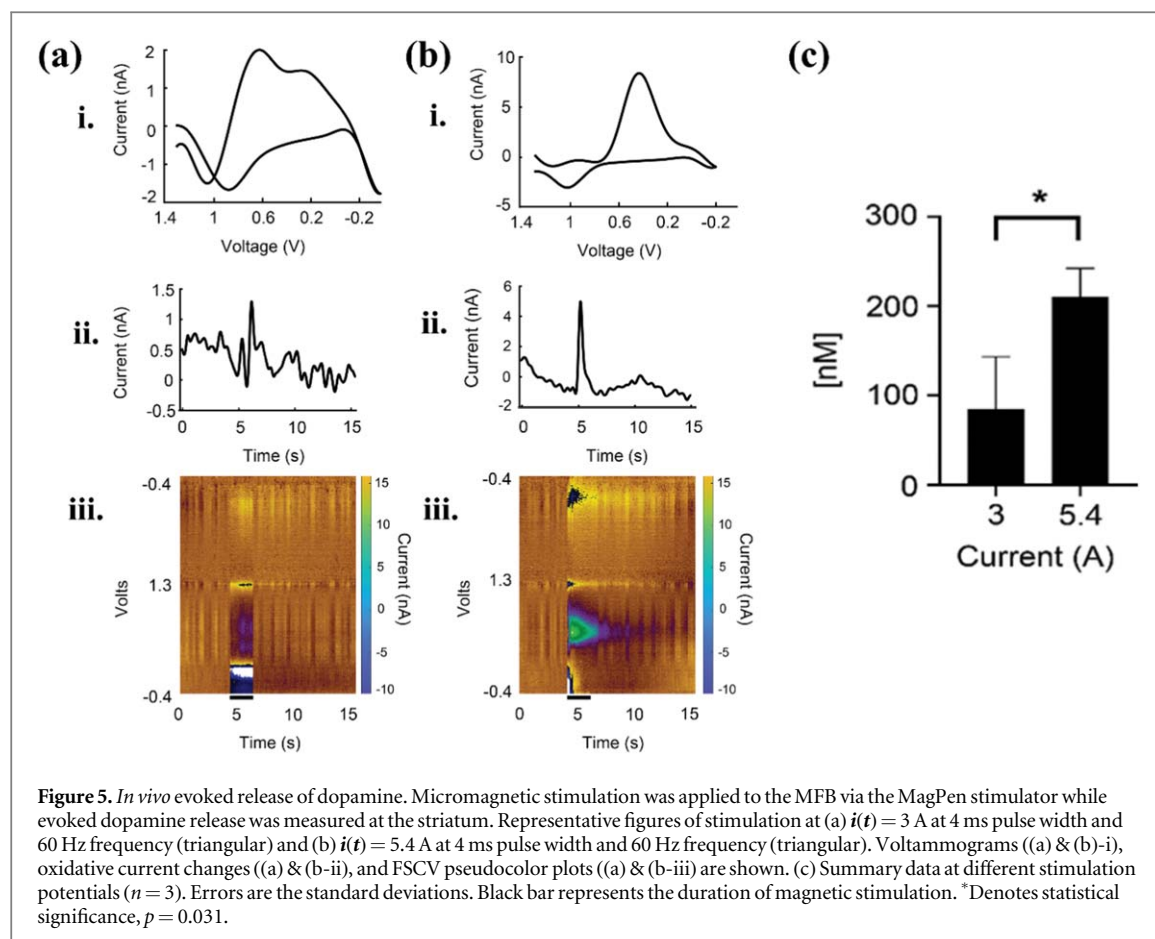
Figure 5. *In vivo* evoked release of dopamine. Micromagnetic stimulation was applied to the MFB via the MagPen stimulator while evoked dopamine release was measured at the striatum. Representative figures of stimulation at (a) $i(t) = 3$ A at 4 ms pulse width and 60 Hz frequency (triangular) and (b) $i(t) = 5.4$ A at 4 ms pulse width and 60 Hz frequency (triangular). Voltammograms ((a) & (b)-i), oxidative current changes ((a) & (b)-ii), and FSCV pseudocolor plots ((a) & (b)-iii) are shown. (c) Summary data at different stimulation potentials ($n = 3$). Errors are the standard deviations. Black bar represents the duration of magnetic stimulation. *Denotes statistical significance, $p = 0.031$.

3.5. Amplitude dependent control of dopamine release

The MagPen-Type H stimulator was tested *in vivo* in a male Sprague-Dawley anesthetized rat (200 g). Briefly, the MagPen was lowered into the right medial forebrain bundle (MFB; coordinates from Bregma in mm: AP −4.6, ML 1.3, DV −8), and the CFM was lowered to the right dorsal striatum (coordinates from Bregma in mm: AP 1.3, ML 2.0, DV −4). Micromagnetic stimulation was applied to the MFB while evoked dopamine release was measured in the dorsal striatum. The stimulation parameters for micromagnetic stimulation were custom calculated to suit the stimulation parameters typically used for FSCV to evoke dopamine release with bipolar electrode stimulation (biphasic square waveform of 300 μA amplitude, 2 ms pulse width and 60 Hz frequency (see figure 3(a))).

The current required to drive the μcoil ($i(t)$) and the corresponding current injected into the brain tissue for dopamine release ($J(t)$) is correlated (see Supplementary Information S2). From our calculations, to inject a current ($J(t)$) of 300–500 μA in to the MFB, we would need the μcoil to drive an approximate current ($i(t)$) between 3 and 5.4 A. Stimulation was delivered at progressively increasing potentials, with the value of $i(t)$ varying from 3 A to 5.4 A (see figures 5(a) and (b)). Representative voltammograms (see figures 5(a-i) and (b-i)), oxidative current traces (see figures 5(a-ii) and (b-ii)), and FSCV pseudocolor plots

(see figures 5(a-iii)) and (b)-(iii) after stimulation at 3 A and 5.4 A are shown in figures 5(a) and (b). Averaging across 3 different trials, it is seen that increasing stimulation amplitude leads to significantly increased dopamine release in the dorsal striatum (paired t-test, 95 nM to 210 nM, $p = 0.031$) (see figure 5(c)).

4. Discussion

This is the first report of micromagnetic stimulation of the MFB fibers *in vivo* to study the evoked dopamine release from the striatum. Micromagnetic stimulation technology is a new neuromodulatory intervention and is still in its infancy. A study of the neurotransmitter release associated with this therapeutic intervention is needed. This work is an early stage study of the same where we used the MagPen as the micromagnetic stimulator to activate the MFB fibers. We studied the *in vivo* evoked dopamine release from the striatum using FSCV. Our study confirmed the importance of the directionality of micromagnetic stimulation. Only one orientation where the long axis of the μcoil is oriented perpendicular to the MFB fibers could successfully activate the MFB fibers to induce dopamine release *in vivo* into the striatum. This orientation could be achieved by MagPen-Type H prototype. Here lies the importance of the directionality of the induced electric field from these μcoils.

In this work, we tried to design the µcoil driving waveforms such that they corroborate those of the electrical stimulation waveforms for MFB activation and dopamine release. Therefore, we designed bursts of triangular waveform of duration 4 ms and 60 Hz frequency such that the induced electric field waveform is a biphasic square waveform of the same duration and frequency. By altering the amplitude of the current driving the µcoil, we could successfully control the *in vivo* dopamine concentration released in the striatum. The concentration of dopamine recorded changed from 95 nM to 210 nM in the striatum when the amplitude of the triangular current through the µcoil was changed from 3 A to 5.4 A.

This work being a proof-of-concept study, there is immense scope of improvement which can pave the path for future studies. A major drawback of the MagPen implant was the bulky dimension of the probe. The MagPen-Type H probe was 1.7 mm in width and 0.4 mm in thickness compared to the bipolar electrodes where each wire had a diameter of 0.127 mm separated by 1 mm. So to insert the MagPen-Type H probe in the MFB of rodent brains *in vivo*, a rectangular hole of length 1.7 mm and width 0.4 mm was required to be drilled. Whereas, to insert the bipolar electrodes in the brain only a hole of length 1.3 mm and width <0.2 mm is usually required to be drilled. Therefore, *in vivo* MagPen insertion in the MFB was an extremely delicate process as it had the possibility to induce rodent brain tissue damage and bleeding. To work around this drawback of the micromagnetic stimulation technology, there is an ardent need for a new design of the µcoil which is fabricated on a flexible material (i.e. there is no density mismatch between the substrate material of the µcoil and the brain tissues). In addition, more efficient µcoils, even µcoil arrays, need to be studied and designed such that they offer more spatially selective activation, thereby improving the focality of micromagnetic neurostimulation even more. Furthermore, as it is unknown if the increase in dopamine concentration with increase in the amplitude of micromagnetic stimulation is linear, this motivates future experiment design in this line of work.

5. Conclusions

We have shown that *in vivo* micromagnetic neurostimulation of the MFB using µcoils of dimension 1 mm × 500 µm × 600 µm can trigger dopamine release from the striatum. The WINCS *Harmoni* system working on the principle of FSCV successfully tracked this dopamine release *in vivo* using carbon fiber microelectrodes (CFM) in real time. Only MagPen-Type H could successfully activate the MFB fibers for dopamine release in the striatum, that too when the long axis of the µcoil was oriented perpendicular to the MFB fibers. Therefore, other than the magnitude of the induced electric field that determines successful

activation of the fibers, the directionality of the induced electric field from these µcoils is also key to successful activation. Furthermore, increasing the amplitude of micromagnetic neurostimulation by 1.8× alters the concentration of dopamine released in the striatum by 2.2×. Overall, this work proves the efficacy of micromagnetic stimulation as an alternative to electrical stimulation in activating the dopamine neurochemical pathway.

Disclosure

The authors and Mayo Clinic (K L, K B, Y O) have a Financial Conflict of Interest in technology used in the research and that the authors and Mayo Clinic may stand to gain financially from the successful outcome of research.

Data availability statement

All data that support the findings of this study are included within the article (and any supplementary files).

ORCID iDs

Renata Saha ⓘ https://orcid.org/0000-0002-0389-0083
Abhinav Goyal ⓘ https://orcid.org/0000-0002-8465-7418
Jason Yuen ⓘ https://orcid.org/0000-0002-6988-388X
Yoonbae Oh ⓘ https://orcid.org/0000-0003-1779-978X
Robert P Bloom ⓘ https://orcid.org/0000-0002-7781-5270
Onri J Benally ⓘ https://orcid.org/0000-0002-8391-9105
Kai Wu ⓘ https://orcid.org/0000-0002-9444-6112
Theoden I Netoff ⓘ https://orcid.org/0000-0002-0115-1930

Walter C Low   https://orcid.org/0000-0001-8593-0175
Kevin E Bennet   https://orcid.org/0000-0003-1715-878X
Kendall H Lee   https://orcid.org/0000-0001-9107-4221
Hojin Shin   https://orcid.org/0000-0001-6095-5122
Jian-Ping Wang   https://orcid.org/0000-0003-2815-6624

References

[1] Jeanneteau F, Funalot B, Jankovic J, Deng H, Lagarde J-P, Lucotte G and Sokoloff P 2006 A functional variant of the dopamine D3 receptor is associated with risk and age-at-onset of essential tremor *Proc. Natl Acad. Sci.* **103** 10753–8

[2] Foley T E and Fleshner M 2008 Neuroplasticity of dopamine circuits after exercise: implications for central fatigue *Neuromolecular Medicine* **10** 67–80

[3] Parsey R V, Oquendo M A, Zea-Ponce Y, Rodenhiser J, Kegeles L S, Pratap M, Cooper T B, Van Heertum R, Mann J J and Laruelle M 2001 Dopamine D2 receptor availability and amphetamine-induced dopamine release in unipolar depression *Biol. Psychiatry* **50** 313–22

[4] Schneier F R, Abi-Dargham A, Martinez D, Slifstein M, Hwang D, Liebowitz M R and Laruelle M 2009 Dopamine transporters, D2 receptors, and dopamine release in generalized social anxiety disorder *Depression and Anxiety* **26** 411–8

[5] Dobryakova E, Genova H M, DeLuca J and Wylie G R 2015 The dopamine imbalance hypothesis of fatigue in multiple sclerosis and other neurological disorders *Frontiers Neurol.* **6** 52

[6] Hélie S, Paul E J and Ashby F G 2012 Simulating the effects of dopamine imbalance on cognition: From positive affect to Parkinson's disease *Neural Netw.* **32** 74–85

[7] Naughton M, Mulrooney J B and Leonard B E 2000 A review of the role of serotonin receptors in psychiatric disorders *Human Psychopharmacology: Clinical and Experimental* **15** 397–415

[8] Wiste A K, Arango V, Ellis S P, Mann J J and Underwood M D 2008 Norepinephrine and serotonin imbalance in the locus coeruleus in bipolar disorder *Bipolar Disorders* **10** 349–59

[9] Lee Y-A, Kim Y-J, Lee J S, Lee S and Goto Y 2021 Imbalance between dopamine and serotonin caused by neonatal habenula lesion *Behavioural Brain Research* **409** 113316

[10] Deuschl G, Beghi E, Fazekas F, Varga T, Christoforidi K A, Sipido E, Bassetti C L, Vos T and Feigin V L 2020 The burden of neurological diseases in Europe: an analysis for the Global Burden of Disease Study 2017 *The Lancet Public Health* **5** e551–67

[11] Lee K H, Lujan J L, Trevathan J K, Ross E K, Bartoletta J J, Park H O, Paek S B, Nicolai E N, Lee J H and Min H-K 2017 WINCS harmoni: closed-loop dynamic neurochemical control of therapeutic interventions *Sci. Rep.* **7** 1–14

[12] Watson C J, Venton B J and Kennedy R T 2006 Vivo measurements of neurotransmitters using microdialysis sampling *Anal. Chem.* **78** 1391–9

[13] Gu H, Varner E L, Groskreutz S R, Michael A C and Weber S G 2015 *In vivo* monitoring of dopamine by microdialysis with 1 min temporal resolution using online capillary liquid chromatography with electrochemical detection *Anal. Chem.* **87** 6088–94

[14] Heien M V, Johnson M A and Wightman R M 2004 *Anal. Chem.* **76** 5697–704

[15] Rodeberg N T, Sandberg S G, Johnson J A, Phillips P E and Wightman R M 2017 Hitchhiker's guide to voltammetry: acute and chronic electrodes for *in vivo* fast-scan cyclic voltammetry *ACS Chem. Neurosci.* **8** 221–34

[16] Kim J, Barath A S, Rusheen A E, Rojas Cabrera J M, Price J B, Shin H, Goyal A, Yuen J W, Jondal D E and Blaha C D 2021 Automatic and reliable quantification of tonic dopamine concentrations *in vivo* using a novel probabilistic inference method *ACS Omega* **6** 6607–13

[17] Robinson D L, Venton B J, Heien M L and Wightman R M 2003 Detecting subsecond dopamine release with fast-scan cyclic voltammetry *in vivo Clin. Chem.* **49** 1763–73

[18] Yuen J, Goyal A, Rusheen A E, Kouzani A Z, Berk M, Kim J H, Tye S J, Blaha C D, Bennet K E and Jang D-P 2021 Cocaine-induced changes in tonic dopamine concentrations measured using multiple-cyclic square wave voltammetry *in vivo Frontiers in Pharmacology* **12** 705254

[19] Bonmassar G, Lee S W, Freeman D K, Polasek M, Fried S I and Gale J T 2012 Microscopic magnetic stimulation of neural tissue *Nat. Commun.* **3** 921

[20] Saha R, Faramarzi S, Bloom R, Benally O J, Wu K, di Girolamo A, Tonini D, Keirstead S A, Low W C and Netoff T 2022 Strength-frequency curve for micromagnetic neurostimulation through excitatory postsynaptic potentials (EPSPs) on rat hippocampal neurons and numerical modeling of magnetic microcoil (μcoil) *J. Neural Eng.* **19** 016018

[21] Saha R, Sanger Z, Bloom R, Benally O, Wu K, Tonini D, Low W C, Keirstead S, Netoff T I and Wang J-P 2023 Micromagnetic stimulation (μMS) dose-response of the rat sciatic nerve *Journal of Neural Engineering* **20** 036022

[22] Jeong H, Cho A, Ay I and Bonmassar G 2022 Short-pulsed micro-magnetic stimulation of the vagus nerve *Frontiers in Physiology* **13** 938101

[23] Lee S W and Fried S I 2014 The response of L5 pyramidal neurons of the PFC to magnetic stimulation from a micro-coil *2014 36th Annual Int. Conf. of the IEEE Engineering in Medicine and Biology Society (IEEE)* pp 6125–8

[24] Park H-J, Bonmassar G, Kaltenbach J A, Machado A G, Manzoor N F and Gale J T 2013 Activation of the central nervous system induced by micro-magnetic stimulation *Nat. Commun.* **4** 2463

[25] Minusa S, Osanai H and Tateno T 2017 Micromagnetic stimulation of the mouse auditory cortex *in vivo* using an implantable solenoid system *IEEE Trans. Biomed. Eng.* **65** 1301–10

[26] Rizou M-E and Prodromakis T 2018 Magnetic stimulation in the microscale: the development of a 6× 6 array of micro-coils for stimulation of excitable cells *in vitro Biomed. Phys. Eng. Express* **4** 025016

[27] Lee S W, Fallegger F, Casse B D and Fried S I 2016 Implantable microcoils for intracortical magnetic stimulation *Sci. Adv.* **2** e1600889

[28] Saha R, Wu K and Wang J-P 2023 Impact of microcoil shape and the efficacy of soft magnetic material cores in focal micromagnetic neurostimulation *2023 11th Int. IEEE/EMBS Conf. on Neural Engineering (NER) (IEEE)* pp 1–4

[29] Saha R, Sanger Z, Bloom R P, Benally O J, Wu K, Tonini D, Low W C, Keirstead S A, Netoff T I and Wang J-P 2023 Micromagnetic stimulation (μMS) dose-response of the rat sciatic nerve *J. Neural Eng.* **20** 036022

[30] Bonmassar G and Serano P 2020 MRI-induced heating of coils for microscopic magnetic stimulation at 1.5 tesla: an initial study *Frontiers in Human Neuroscience* **14** 53

[31] Chang S-Y, Kimble C J, Kim I, Paek S B, Kressin K R, Boesche J B, Whitlock S V, Eaker D R, Kasasbeh A and Horne A E 2013 Development of the mayo investigational neuromodulation control system: toward a closed-loop electrochemical feedback system for deep brain stimulation *Journal of Neurosurgery* **119** 1556–65

[32] Oh Y, Park C, Kim D H, Shin H, Kang Y M, DeWaele M, Lee J, Min H-K, Blaha C D and Bennet K E 2016 Monitoring *in vivo* changes in tonic extracellular dopamine level by charge-balancing multiple waveform fast-scan cyclic voltammetry *Anal. Chem.* **88** 10962–70

[33] Oh Y, Heien M L, Park C, Kang Y M, Kim J, Boschen S L, Shin H, Cho H U, Blaha C D and Bennet K E 2018 Tracking tonic dopamine levels *in vivo* using multiple cyclic square wave voltammetry *Biosens. Bioelectron.* **121** 174–82

[34] Paxinos G and Watson C 2007 *The Rat Brain in Stereotaxic Coordinates.* (Elsevier Inc.)

[35] Clark J J, Sandberg S G, Wanat M J, Gan J O, Horne E A, Hart A S, Akers C A, Parker J G, Willuhn I and Martinez V 2010

Chronic microsensors for longitudinal, subsecond dopamine detection in behaving animals *Nat. Methods* **7** 126–9

[36] Martyanov A S and Neustroyev N I 2014 ANSYS maxwell software for electromagnetic field calculations *Eastern European Scientific Journal* **5**

[37] Ren Z 2002 T-/spl omega/formulation for eddy-current problems in multiply connected regions *IEEE Trans. Magn.* **38** 557–60

[38] Venton B J and Cao Q 2020 Fundamentals of fast-scan cyclic voltammetry for dopamine detection *Analyst* **145** 1158–68

[39] Bosman L W, Houweling A R, Owens C B, Tanke N, Shevchouk O T, Rahmati N, Teunissen W H, Ju C, Gong W and Koekkoek S K 2011 Anatomical pathways involved in generating and sensing rhythmic whisker movements *Frontiers in Integrative Neuroscience* **5** 53

[40] Golestanirad L, Gale J T, Manzoor N F, Park H-J, Glait L, Haer F, Kaltenbach J A and Bonmassar G 2018 Solenoidal micromagnetic stimulation enables activation of axons with specific orientation *Frontiers in Physiology* **9** 724